# Oxygen vacancy formation on clean and hydroxylated low-index $V_2O_5$ surfaces: A density functional investigation

Jakub Goclon,[1] Robert Grybos,[1,2,*] Małgorzata Witko,[1] and Jürgen Hafner[2]
[1]*Institute of Catalysis and Surface Chemistry PAS, Niezapominajek 8, 30-239 Kraków, Poland*
[2]*Fakultät für Physik and Center for Computational Materials Science, Universität Wien, Sensengasse 8/12, A-1090 Wien, Austria*
(Received 17 August 2008; revised manuscript received 11 December 2008; published 25 February 2009)

We present *ab initio* density functional studies of the stability and the formation of oxygen vacancies on three low-index surfaces of $V_2O_5$. In agreement with the experimental results on the morphology of $V_2O_5$ crystallites we find that the surface energies of the (100) and (001) surfaces are considerably higher than that of the (010) surface such that in equilibrium 85% of the surface area is occupied by (010) surfaces. However, we also find that the energies required for the formation of oxygen vacancies are considerably lower on the energetically less favorable surfaces. As reported in earlier theoretical studies we find that on the (010) surface, the elimination of an oxygen atom from the vanadyl group [denoted O(1)] requires considerably less energy ($E_f$=4.7 eV relative to atomic oxygen) than the formation of a vacancy by desorption of twofold or threefold coordinated O(2) and O(3) oxygen atoms ($E_f$=6.5 eV). In addition, the thermodynamic analysis shows that under conditions required for vacancy creation (very low value of the oxygen partial pressure) the $V_2O_5$ phase is unstable and may transform into $VO_2$ by releasing molecular oxygen. Due to extensive framework relaxation, the formation of vacancies at the O(1) and O(2) sites of the (001) and (100) surfaces requires 1.0–1.5 eV less energy than on the (010) surface. A thermodynamic analysis demonstrates that on the (010) surfaces only O(1) vacancies are marginally stable against reoxidation under strongly reducing conditions, while on the (100) and (001) surfaces all types of vacancies are stable even under much higher partial pressures of oxygen. In addition, the adsorption of atomic hydrogen and the formation of hydroxyl groups had been studied on all three surfaces. Hydrogen adsorption is an exothermic process. Adsorption energies on vanadyl O(1) atoms are larger by about 1.1 and 1.6 eV on the (001) and (100) surfaces than on the (010) surface and adsorption energies on O(2) sites are larger by 0.8–1.2 eV. Vacancy formation by elimination of a hydroxyl group requires less energy than abstraction of an oxygen atom. On the (010) surface the vacancy formation energies are reduced by 1.6–1.7 eV; on the (001) and (100) surfaces the reduction varies between 0.1 and 0.9 eV. However, the lowest vacancy formation energies are still 3.1 eV on the (010) and 2.9 and 2.3 eV on the (001) and (100) surfaces, respectively. The lower vacancy formation energies mean that although in equilibrium only about 15.5% of the surface area of a crystallite consists of (001) and (100) facets, these surfaces will make a considerable contribution to the activity of $V_2O_5$ as an oxidation catalyst.

DOI: 10.1103/PhysRevB.79.075439 PACS number(s): 31.15.A−, 82.65.+r

## I. INTRODUCTION

Selective catalytic oxidation is a very important process in the production of alcohols, aldehydes, ketones, and acids. These reactions proceed according to the Mars–van Krevelen mechanism[1] in which the formation of a surface oxygen vacancy is an essential process. Hence the activity and selectivity of an oxidation catalyst, such as vanadium pentoxide, depends on the ability to provide surface oxygen as a reactant, i.e., on the energy of vacancy creation. A low energy of vacancy creation increases the catalytic activity, but it may also decrease the selectivity to partial oxidation products and favor total oxidation. Creation of surface oxygen vacancies might also become the starting point for other processes such as creation of linear/planar defects or shear planes and can eventually lead to a total reduction in the oxide.[2]

A dependence of catalytic properties on the crystallographic structure of an exposed surface, called the "crystallographic anisotropy," was first observed for metal catalysts,[3] but a similar behavior was also reported for metal oxide catalysts.[4,5] Volta and Tatibouet[6] investigated the catalytic activity of $MoO_3$ crystals for the oxidation of alkenes and showed that the (100) face is active and selective for allylic oxidation, while the (010) plane is specific for complete oxidation. Gąsior and Machej[7] demonstrated that selective oxidation of o-xylene to phthalic anhydride depends on the morphology of the $V_2O_5$ grains. Higher selectivity is observed for vanadia particles with a higher fraction of (010) facets. Similarly, the reduction in isopropanol to propene or acetone depends on the morphology of the $V_2O_5$ crystal. The selectivity to acetone increases with a higher percentage of (010) planes in the total crystallite surface area, whereas the selectivity to propene decreases.[8] However, to date very little is known about the properties of $V_2O_5$ surfaces other than (010). Therefore, it seems worthwhile to study the reactivity of different low-index surfaces of $V_2O_5$, as quantified by the energies for oxygen vacancy creation.

Scanning tunneling microscopy (STM) (Ref. 9) and atomic force microscopy (AFM) (Refs. 10 and 11) show that $V_2O_5$ crystallites form thin platelets, exposing mostly (010) surfaces with coordinatively saturated surface atoms. Consequently, theoretical investigations of $V_2O_5$ surfaces using cluster and periodic models have concentrated exclusively on the most stable (010) surface. Only a few of the periodic studies were extended to oxygen vacancy creation.[12–14] Ganduglia-Pirovano and Sauer[13] investigated the formation

 

of vacancies on the (010) surfaces and the stability of the reduced surfaces. It was demonstrated that the vacancy formation energy is lowest for the vanadyl oxygen atoms O(1), whose desorption leads to a strong relaxation of the surface. The formation of interlayer bonds between a vanadium atom and a vanadyl oxygen in a subsurface layer helps to reduce the vacancy formation energy. Alignment of neighboring O(1) vacancies in the [001] direction permits an additional reduction in the energy. Vacancy creation by elimination of O(2) or O(3) atoms leads to more modest relaxation effects and requires significantly higher energies. Subsequent work of the same group[14] showed that the situation is very similar for the $\gamma$ phase of $V_2O_5$. Yin *et al.*[12] studied the adsorption of atomic hydrogen at oxygen atoms on the $V_2O_5$ (010) surface and the formation of vacancies by elimination of the hydroxyl group. It was demonstrated that, if relaxation is taken into account, only very small differences exist in the adsorption energies at nonequivalent oxygen sites. The energetic cost for the elimination of a hydroxyl group is lowest for the O(3) site, but this result has to be considered with some reserve because no relaxation of the surface was allowed. Fu *et al.*[15] examined the oxidative dehydrogenation of propane over the $V_2O_5$ (010) surface and concluded that the vanadyl oxygen is more reactive than the O(2) atom in C–H bond activation and that the O(3) site is inert. However, the i-propoxide formed at the O(1) site is very stable against further decomposition to propene, whereas on the O(2) site it is more easily transformed. These results demonstrate that the specific chemical reactivity is strongly dependent on the geometry of the reactive site.

In the present work we extend the investigations of the surface energetics and of the formation of various types of oxygen vacancies to the less stable (100) and (010) surfaces [for comparison also results on the (010) surface are presented]. We demonstrate that although in equilibrium the (100) and (001) surfaces occupy only about 15% of the total surface area of a crystallite, the creation of oxygen vacancies on these surfaces requires between 1.0 and 1.5 eV less energy than on the dominant (010) surface. In addition, we study the hydroxylation of all three surfaces by adsorption of atomic hydrogen and the creation of vacancies by the abstraction of hydroxyl groups. The results of our calculations show that hydrogen adsorption is more exothermic on the unsaturated (001) and (100) than on the saturated (010) surface. Therefore the differences in the energies for vacancy formation via dehydroxylation are less dramatic than by direct oxygen desorption. However, vacancy formation on the (001) and (100) surfaces still requires between 0.1 and 0.9 eV less energy than on the (010) surface. These results suggest that the (100) and (001) surfaces (which form the thin edges of $V_2O_5$ platelets) may play a significant role in the activity of vanadium pentoxide as an oxidation catalyst.

## II. METHODOLOGY

### A. *Ab initio* density functional calculations

Periodic *ab initio* density functional calculations were carried out using Vienna Ab-initio Simulation Package (VASP) (Ref. 16) with the semilocal exchange-correlation functional PW91.[17] The projector-augmented wave (PAW) method was used together with a plane wave basis set with 600 eV cutoff. All calculations were spin polarized.

Vanadium pentoxide forms layered crystals with strong covalent bonding between the atoms in a layer and weak van der Waals bonding between the layers. It is well known that dispersion (van der Waals) forces are not properly accounted for by density functional theory (DFT). An attempt to apply semiempirical long-range dispersion corrections[18] to $V_2O_5$ was recently made by Kerber *et al.*[19] An optimization of the lattice constant $b$ in the direction perpendicular to the layers (with the lattice constants $a$ and $c$ fixed at their DFT values) leads to an improved prediction of the interlayer distance. We shall return to this point below.

One should also mention that the application of local and semilocal exchange-correlation functionals to problems such as defect formation in transition-metal oxides or on their surfaces was sometimes criticized[20] and the use of post-DFT methods such as DFT+$U$ or hybrid functionals was recommended. This critique is undoubtedly justified for systems where DFT predicts a much narrower band gap than experimentally measured and where indeed the DFT+$U$ method[21] or hybrid functionals[22] significantly improve predictions. For $V_2O_5$ however, the predicted band gap is only marginally lower than the experimental estimate (details are given below) and it appears to be legitimate to use the gradient-corrected PW91 functional and to avoid the huge computational effort associated with hybrid-functional calculations for large systems.

Supercells for surface calculations are constructed by repeating the bulk unit cell along the $a$, $b$, and $c$ lattice vectors and adding a vacuum region wide enough to avoid surface-surface interactions (10–15 Å). Both sides of the periodically repeated slabs expose the same surface. For each surface, supercells of three sizes, corresponding to different concentrations of surface vacancies, were used. Actual sizes, along with the $k$-point meshes used for Brillouin-zone integrations, are given in Sec. II B describing the surface models.

The relaxation of ionic positions was carried out using a conjugate-gradient algorithm. For the slab models of the (010) surface, positions of all atoms were allowed to relax, while for models representing the (001) and (100) surfaces only three and four top layers, respectively, were relaxed, while the inner part of the slab was kept frozen in a bulklike geometry. It was checked that freezing deeper layers have no influence on the surface geometry. The convergence criteria for electronic and geometrical structures were set to $10^{-5}$ and $10^{-4}$ eV, respectively.

### B. Thermodynamic stability of surfaces

The chemical composition and geometry of a $V_2O_5$ surface in contact with an oxygen reservoir at given temperature $T$ and oxygen partial pressure $p$ is determined by the minimum of the surface free energy $\gamma(T,p)$ defined in the grand-canonical ensemble as[23,24]

$$\gamma(T,p) = [G(T,p,N_V,N_O) - N_V\mu_V(T,p) - N_O\mu_O(T,p)]/A, \quad (1)$$

where $G(T,p,N_V,N_O)$ is the Gibbs free energy of the model of the surface, $\mu_V(T,p)$ and $\mu_O(T,p)$ are the chemical poten-

tials of V and O atoms, and $A$ is the surface area. In equilibrium with the bulk they are related by the condition $4\mu_V(T,p)+10\mu_O(T,p)=G_{V_2O_5}(T,p)$, where $G_{V_2O_5}(T,p)$ is the Gibbs free energy per $V_2O_5$ elementary cell containing 2 f.u. Neglecting atomic vibrations, the Gibbs free energy of the surface $G(T,p,N_V,N_O)$ may be approximated by the internal energy $E_{slab}(N_V,N_O)$ of the slab model representing the surface and the Gibbs free energy of the bulk crystal by the total energy per elementary cell $E_{bulk}$, both determined by DFT total-energy calculations, so that finally

$$\gamma(T,p) = [E_{slab}(N_V,N_O) - N_V E_{bulk}/4 - (10N_V/4 - N_O)\mu_O(T,p)]/A. \quad (2)$$

A lower limit to the oxygen chemical potential is determined by the value where $V_2O_5$ becomes unstable against reduction to $VO_2$, the upper limit by the onset of condensation of molecular oxygen on the surfaces, i.e., the oxygen chemical potential $\mu_O(T,p)$ is limited to the interval

$$[E_{bulk}(V_2O_5) - 2E_{bulk}(VO_2)]/2 < \mu_O(T,p) < E(O_2)/2, \quad (3)$$

where $E(O_2)$ is the cohesive energy of an $O_2$ molecule as calculated using DFT.

### C. Surface energy and crystallite morphology

The equilibrium morphology of crystallites may be determined using the Wulff method.[25] The distances $d_{hkl}$ of facets with the orientation $(hkl)$ from the crystal's center are proportional to their surface energies,

$$d_{ijk}:d_{lmn} = E_{surf}(ijk):E_{surf}(lmn). \quad (4)$$

Equation (4) allows us to determine the contribution of the surfaces of different orientations to the total surface area of a crystallite.

### D. Energy of vacancy formation

Experimentally, the energy for O-vacancy formation can be estimated from conductivity measurements. For a $V_2O_5$ (010) surface values ranging between 1.3 and 1.5 eV have been reported.[26] Theoretically, the formation energy of an isolated oxygen vacancy $E_f(O)$ can be defined as

$$E_f(O) = E(V_xO_{y-1}) + E(O) - E(V_xO_y), \quad (5)$$

i.e., the difference between the total energy of a cell containing an isolated vacancy $E(V_xO_{y-1})$ plus the energy $E(O)$ of an isolated oxygen atom and the energy of the cell without the vacancy $E(V_xO_y)$. Alternatively, a gas-phase oxygen molecule could be taken as a reference. In this case the calculated vacancy formation energy is reduced by a half of the binding energy per $O_2$ molecule, i.e., by $\frac{1}{2}E(O_2)=3.13$ eV.

Under realistic conditions, hydroxyl groups cover the oxide surface. The adsorption energy of atomic hydrogen $E_{ads}(H)$ on various oxygen sites can be estimated as the difference between the total energy $E(V_xO_yH)$ of the relaxed hydroxylated surface and the sum of the total energy

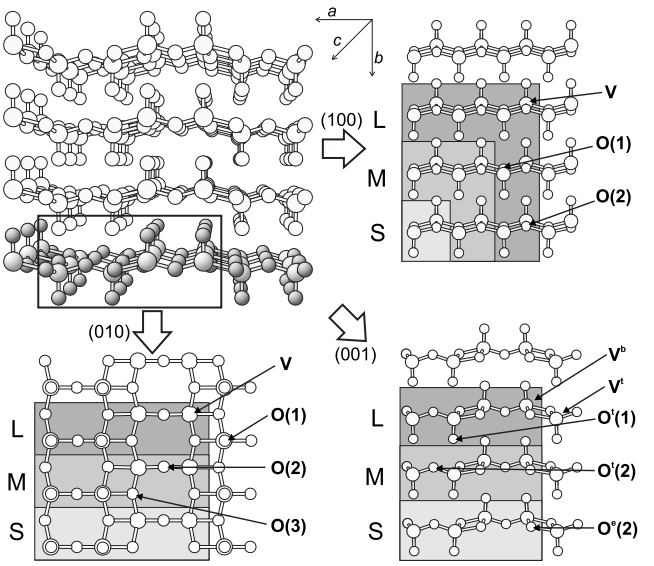


FIG. 1. Perspective view of the crystal structure of $V_2O_5$ and top view of the three low-index surfaces: (010), (001), and (100). Large spheres represent V; small spheres O atoms. The black frame shows the bulk unit cell, the shaded areas the large (L), medium (M), and small (S) surface cells. Oxygen atoms with one, two, or three V neighbors are marked as O(1)–O(3). For the (001) surface $O^t(1)$ and $O^t(2)$ mark oxygen atoms located on the plateaus and $O^e(2)$ oxygen atoms on the edge of the plateau (cf. text).

$E(V_xO_y)$ of the clean surface and the energy of an isolated hydrogen atom $E(H)$,

$$E_{ads}(H) = E(V_xO_yH) - E(V_xO_y) - E(H). \quad (6)$$

The energy required for the elimination of an OH group is lower than that for the abstraction of an oxygen atom alone because the hydroxyl group is not as strongly bound and it is more stable in the gas phase. The formation energy of a vacancy by elimination of a hydroxyl group is defined as

$$E_f(OH) = E(V_xO_{y-1}) + E(OH) - E(V_xO_yH), \quad (7)$$

where $E(V_xO_{y-1})$ is the energy of a supercell with a vacancy, $E(OH)$ is the energy of an isolated hydroxyl group, and $E(V_xO_yH)$ is the energy of a cell where a hydrogen atom is adsorbed at one of the oxygen atoms.

## III. STRUCTURE AND STABILITY OF $V_2O_5$ SURFACES

### A. Bulk $V_2O_5$

Vanadium pentoxide crystallizes in an orthorhombic lattice (space group $D_{2h}$-$P_{mmm}$, $a=11.51$ Å, $b=4.37$ Å, and $c=3.56$ Å). The unit cell contains two stoichiometric $V_2O_5$ units.[27,28] Note that the lattice vectors $b$ and $c$ are sometimes interchanged and in the following notation of Bachmann *et al.*[27] where $b>c$ is used.

$V_2O_5$ has a layered structure with a cleavage plane parallel to (010) (see Fig. 1). All atoms on the (010) surface of a layer are coordinatively saturated; bonding between layers is provided by van der Waals forces. To avoid confusion, the coordinatively saturated (010) surfaces will be called "s lay-

ers." van der Waals interactions are underestimated by DFT methods. Even after a very careful optimization of the bulk structure, resulting in $a=11.65$ Å, $b=4.66$ Å, and $c=3.57$ Å, the lattice constant $b$ is overestimated by about 6.6%, which is in excellent agreement with the work of Kresse *et al.*[29] based on the same method. Other calculations (also using the same approach) report values of $b$ varying between 4.47 and 4.84 Å.[13,30] The reason for this discrepancy is that the potential-energy surface is very flat in the $b$ direction, so that very strict convergence criteria need to be applied.

In bulk $V_2O_5$ there are three different types of oxygen atoms: (i) singly coordinated terminal (vanadyl) oxygen atoms denoted as O(1) [V–O(1) bond length 1.61/1.58 Å in theory/experiment], (ii) doubly coordinated bridging oxygen atoms denoted as O(2) which are connected to two neighboring vanadium centers with bonds of equal length (1.79/1.78 Å in theory/experiment), and (iii) triply coordinated bridging oxygen atoms denoted as O(3) bonded to two vanadium atoms with short bonds (1.89/1.88 Å in theory/experiment) and one with a long bond (2.05/2.02 Å in theory/experiment). There is also a very long bond between the vanadium atoms in one s layer and an O(1) oxygen from the neighboring s layer. The calculated bond length is 3.06 Å compared to an experimental value of 2.79 Å. Note that the error in the calculated lattice constant $b$ is 0.29 Å. The comparison shows that the failure of DFT to account for the van der Waals forces affects only the interlayer distance while the internal structure of the s layers is described very accurately. Details of the structural optimization of bulk $V_2O_5$ will be reported elsewhere.[31]

The analysis of the electronic structure shows that $V_2O_5$ is a semiconductor with a direct gap of $E_g=2.19$ eV [in good agreement with experimental estimates based on photodesorption experiments[32] ($E_g=2.35$ eV), optical adsorption[33] ($E_g=2.30$ eV), and optical reflectance[34] ($E_g=2.38$ eV)]. The indirect band of 1.92 eV is slightly lower. The good agreement of the band gaps calculated with the PW91 functional confirms that gradient-corrected exchange-correlation functionals provide an adequate description of the electronic structure, which is an important assessment of the validity of this approach for calculating vacancy formation energies.

### B. (010) surface structure and surface energy

In Sec. III C we present the structure models used for the description of the low-index surfaces. Schematic representations are shown in Fig. 1. We begin with the (010) surface. The slab model consists of two s layers linked by van der Waals forces. To model the surface three surface supercells were used: $(1\times2\times1)$ (small—S), $(1\times2\times2)$ (medium—M), and $(1\times2\times3)$ (large—L) containing 28, 56, and 84 atoms, respectively. For the S cell, a $(2\times1\times6)$ $k$-point mesh was used for Brillouin-zone integrations, while for the two larger cells the Γ point was sufficient. The supercells have surface areas of 0.42, 0.83, and 1.25 nm$^2$, respectively. In each supercell, only one surface oxygen vacancy was created. The minimal distances between a vacancy and its periodically repeated image are 3.57, 7.14, and 10.71 Å for S, M, and L cells, respectively.

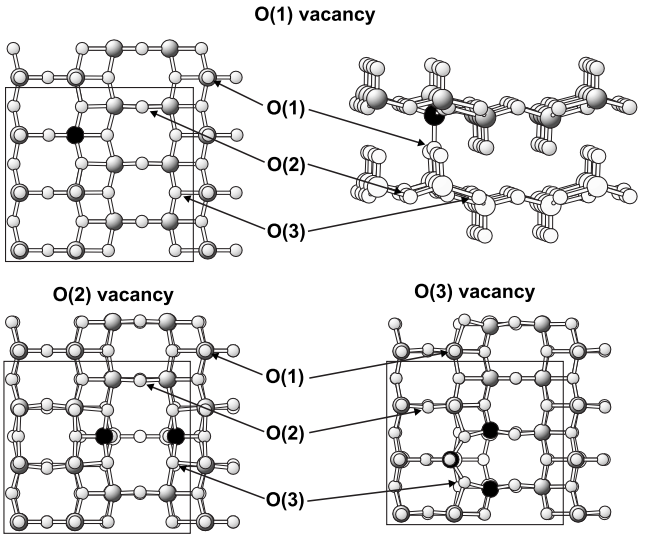


FIG. 2. Relaxed geometries around O(1), O(2), and O(3) vacancies on the (010) surface (for the L supercell). Structures are presented in top view, except for the O(1) vacancy, where a side view depicts the formation of a new bond between surface and subsurface s layers. For clarity, V*—the vanadium atoms which were bonded to the removed O atom are depicted in solid black.

On a $V_2O_5$ (010) surface three nonequivalent oxygen sites are accessible to adsorbing molecules: O(1), O(2), and O(3) as described for the bulk (see Fig. 2). Due to surface cleavage, two additional centers are present: O′(2) and O′(3) sites located between vanadyl groups sticking out of the surface. Since they are not easily accessible from the gas phase because of sterical hindrance, they will not be taken into consideration.

Because of the weak interaction between adjacent s layers surface relaxations are very modest; details are given in Ref. 31. The $d_{\text{V-O(1)}}$ distances are the same as in the bulk whereas the $d_{\text{V-O(2)}}$, $d_{\text{V-O′(2)}}$, $d_{\text{V-O(3)}}$, and $d_{\text{V-O′(3)}}$ bond lengths are larger only by 0.02, 0.02, 0.01, and 0.01 Å, respectively. The surface energy of the $V_2O_5$ (010) surface is very low even for an unrelaxed bulk-terminated geometry ($E_{\text{surf}}=0.054$ J/m$^2$). If a full relaxation is allowed, this value is reduced to 0.047 J/m$^2$. Our results for geometric relaxation and for the surface energy agree very well with Ganduglia-Pirovano and Sauer[13] where surface energies of 0.048 and 0.040 J/m$^2$ for the unrelaxed and relaxed surfaces, respectively, have been reported.

### C. (001) surface structure and surface energy

For the (001) surface $(1\times1\times4)$, $(1\times2\times4)$, and $(1\times3\times4)$ supercells were used (see Fig. 1), separated along the $c$ direction by a vacuum region with a thickness corresponding to four bulk unit cells. The small cell contains 56 atoms; for Brillouin-zone integrations a $(2\times6\times1)$ $k$ mesh was used. Medium and large cells consist of 112 and 168 atoms, respectively, and were described by the Γ point only. The surface areas of the three cells are 0.54, 1.09, and 1.63 nm$^2$, and the minimal vacancy-vacancy distances are 4.66, 9.32, and 13.98 Å for the small, medium, and large cells, respec-

tively. The s layers are perpendicular to the surface and this leads to a strong surface relaxation.

The $V_2O_5$ (001) surface is strongly corrugated, with alternating "plateaus" and "valleys." Oxygen atoms are located on top of the plateau (t), at its edge (e), or at the bottom (b) of the valley. Hence five different oxygen atoms can be identified: $O^t(1)$, $O^t(2)$ on the plateau, $O^e(2)$ on the edge, and $O^b(1)$, $O^b(2)$ in the valley. The last two sites were not considered as they are not easily accessible from above the surface (see Fig. 1). One should note that there are no triply coordinated oxygen atoms O(3) on the (001) surface. Cleavage along a (001) plane breaks one of the O(3)–V bonds, thus the bulk O(3) atom becomes an $O^e(2)$ site at the surface. Also the vanadium atoms are not all equivalent: $V^t$ atoms on the plateau are linked to another $V^t$ by an $O^t(2)$ atom, while $V^b$ are located in a valley, below the edge of the plateau, and similarly are coupled by $O^b(2)$ atoms.

The formation of this surface requires breaking of strong V–O bonds; hence the surface energy for a nonrelaxed structure is large, 1.16 $J/m^2$, for the 56-atom supercell. This value is well converged with respect to the size of the cell. Relaxation leads to a dramatic reduction in the surface energy to 0.48 $J/m^2$. The V–O(1) bond length is 1.61 Å, which is equal to its value in the bulk. The bond lengths $V^t$-$O^t(2)$ and $V^t$-$O^e(2)$ (on the plateau) vary from 1.79 (this is also the bulk value) to 1.83 Å. The strongest changes are observed for bonds linking $V^b$ and O(3) lying directly below; they are stretched to 4.09 Å, compared to 3.57 Å in the bulk. In contrast, the bonds $V^t$-O(3) are contracted by 0.12–0.13 Å. Due to the layer-type character of $V_2O_5$ some changes in bond lengths appear also in deeper layers, but they never exceed 0.06 Å.

### D. (100) surface structure and surface energy

A (100) surface may be created by cutting the crystal at different planes. In our previous work four different terminations were tested.[31] A termination exposing at the surface a V atom linked to two O atoms, an O(1) atom from a vanadyl group and a twofold coordinated O(2) atom [corresponding to an O(3) atom in the bulk], was found to have the lowest surface energy over the entire admissible range of chemical potentials. This termination produces also a stoichiometric slab. For the calculation of vacancy formation energies the (100) surface was described by $(1\times1\times1)$, $(1\times2\times2)$, and $(1\times3\times3)$ supercells containing 14, 56, and 126 atoms, respectively (see Fig. 1). The surface areas of these cells are 0.17, 0.67, and 1.50 $nm^2$, and the minimal vacancy-vacancy distances are 3.57, 7.14, and 10.71 Å for small, medium, and large cells, respectively. The slab thickness corresponds to the size of the bulk unit cell along the $a$ direction ($a$ =11.65 Å). At the (100) surface only onefold and twofold coordinated oxygen atoms, denoted as O(1) and O(2), are present and all surface vanadium centers are equivalent (see Fig. 1). The surface energies are 0.61 $J/m^2$ for the unrelaxed surface and 0.55 $J/m^2$ for the relaxed surface. The changes in the surface structure induced by relaxation are modest.[31]

### E. Equilibrium morphology of $V_2O_5$ crystallites

For relaxed geometries, the surface energies of the low-index $V_2O_5$ surfaces are 0.047, 0.48, and 0.55 $J/m^2$ for the (010), (001), and (100) surfaces, respectively. In the equilibrium morphology determined by the Wulff construction[25] the saturated (010) surface occupies 84.5% of the total surface area of a $V_2O_5$ crystallite, while the other two unsaturated surfaces contribute only 15.5%. If empirical corrections for the van der Waals interaction between the saturated layers were applied, the surface energy of the (010) surface would increase, while that of the other low-index surfaces can be expected to remain largely unaffected. Hence the percentage of (100) and (001) facets exposed on the crystal surface can only increase. The theoretical crystal shape is similar to the platelets seen in scanning electron microscopy (SEM).[10,11] However, if the formation of oxygen vacancies requires a lower energy on these unsaturated surfaces compared to the saturated (010) surface, these surfaces may still play an important role in oxidation catalysis. A similar situation is observed for the layered transition-metal sulfides (e.g., $MoS_2$) used as catalysts in hydrodesulphurization where it is accepted that active sites exist only at the edges of the layers.[35,36]

### F. Reduced low-index surface structures and energies

Ground-state energies of the reduced surfaces were calculated for an unrelaxed geometry as optimized for the stoichiometric surfaces and also after allowing a full relaxation around the created vacancy. Table I summarizes the vacancy formation energies for different types of vacancies on the (010), (001), and (100) surfaces, as calculated using small, medium, and large supercells. Relaxation effects, expressed by the relaxation energy $E_{\mathrm{relax}}$ (with negative values as relaxation lowers the total energy), are found to be rather large and dependent on the surface orientation and on the size of the supercell (vacancy concentration). All vacancy calculations were performed in a spin-polarized mode; for all cases the ground state is a triplet state.

### G. Reduced (010) surface

The formation energies of O(1), O(2), and O(3) oxygen vacancies on the (010) surface are compiled in Table I. The formation energy (with respect to atomic oxygen) is lowest for the vanadyl oxygen atoms O(1) [$E_f$=4.72 eV for the large relaxed cell]. Vacancy formation is favored by a strong relaxation leading to an energy gain of $E_{\mathrm{relax}}$=−1.94 eV. Relaxation leads to the formation of a bond between saturated s layers: the $V^*$ atom (the one next to the vacancy site—shown in solid black in the following figures) shifts inward and creates a bond with an O(1) atom from the next s layer. As a result the $V^*$-O(1) distance is reduced from 3.06 to 1.77 Å and the V–O(1) bond in the second s layer is expanded from 1.61 to 1.76 Å. This scenario is a characteristic feature of vacancy-induced surface relaxation also on the other surfaces. Formation of O(2) and O(3) vacancies requires much higher energies of 6.47 and 6.64 eV, respectively. The contribution of the surface relaxation is also much weaker, 1.52 and 0.74 eV for the large cell.

Both vacancy formation and relaxation influence the oxidation state of the vanadium atom. In the bulk and at the stoichiometric surface, the formal oxidation state of vana-

TABLE I. Energies of vacancy formation for the three low-index surfaces of $V_2O_5$, $E^R_{f(O)}$, relative to atomic oxygen (formation energies relative to molecular oxygen are given in parentheses); $E_{relax}$ is the relaxation energy. All values are given in eV. Three different supercell sizes were used: small (S), medium (M), and large (L), leading to different vacancy concentrations as discussed in the text.

| | | (010) | | | (001) | | | (100) | |
|---|---|---|---|---|---|---|---|---|---|
| | Energy | O(1) | O(2) | O(3) | O(1) | O(2) | O$^e$(2) | O(1) | O(2) |
| S | $E^R_{f(O)}$ | 4.81(1.68) | 7.12(3.99) | 7.27(4.14) | 6.30(3.17) | 7.58(4.45)9 | 6.62(3.49) | 6.40(3.27) | 7.89(4.76) |
| | $E_{relax}$ | −1.90 | −0.98 | −0.54 | −0.55 | −0.85 | −1.16 | −0.38 | −0.18 |
| M | $E^R_{f(O)}$ | 4.83(1.70) | 6.88(3.75) | 7.42(4.29) | 3.54(0.41) | 3.71(0.58) | 3.51(0.38) | 4.42(1.29) | 4.39(1.26) |
| | $E_{relax}$ | −1.79 | −1.37 | −0.64 | −3.30 | −4.62 | −4.42 | −2.28 | −3.77 |
| L | $E^R_{f(O)}$ | 4.72(1.69) | 6.47(3.34) | 6.64(3.51) | 3.83(0.70) | 3.87(0.84) | 3.88(0.85) | 3.46(0.33) | 3.19(0.06) |
| | $E_{relax}$ | −1.94 | −1.52 | −0.74 | −3.02 | −4.42 | −3.85 | −3.30 | −4.63 |

dium is $V^{5+}$, creation of a neutral vacancy without relaxation changes the formal oxidation state to $V^{3+}$, whereas relaxation and formation of a new V–O(1) bond alter the formal oxidation state of both V atoms sharing the O(1) atom to $V^{4+}$. Hence the relaxation leads to a distribution of the excess charge created by vacancy formation over neighboring metal atoms. Whereas the V–O(1) bond in a vanadyl group is a double V=O bond, the two new V–O bonds are single bonds. In the bulk and at the stoichiometric surface, five oxygen atoms coordinate V in a square-pyramidal arrangement. After creation of the O(1) vacancy and relaxation, the $V^*$ atom (located next to the vacancy site) is again fivefold coordinated (see Fig. 2), but the square pyramid is inverted and shares an O vertex with a pyramid around a V atom in the next s layer. The distances between the $V^*$ atoms and the four O atoms in the nearly square basal planes of the pyramid are slightly reduced to 1.71 [V-O′(2)], 1.85 [V-O′(3)], and 2.02 [V–O(3)] Å compared to 1.81, 1.90, and 2.06 Å on the unrelaxed surface and to 1.79, 1.89, and 2.05 Å in the bulk. The V-O(2)-$V^*$ angles are stretched from 150° to nearly 180°.

Relaxations around the O(2) and O(3) vacancies follow a very different pattern. Elimination of an O(2) oxygen atom leads to an undercoordination of two V atoms (see Fig. 2); the $V^*$-O(3) and $V^*$-O′(3) bonds around these atoms are contracted by up to −0.19 Å, while the length of the vanadyl bond pointing toward the bulk is slightly stretched by 0.07 Å. The strong back bonds draw the undercoordinated vanadium atoms apart; their distance increases by more than 1 Å. Increasing the supercell size leads to an increase in the relaxation energy from −0.98 to −1.52 eV because for a larger distance between the vacancies less constraints are imposed on the relaxation.

Creation of an O(3) vacancy results in an undercoordination of three V atoms, one with a vanadyl group pointing away from the surface and two with $V^*$-O(1) bonds pointing toward the bulk (see Fig. 2). Again, due to the formation of back bonds, the distance between the undercoordinated $V^*$ atoms increases and the $V^*$-O(3) and $V^*$-O′(3) bonds are shortened by 0.12 and 0.15 Å, respectively. Relaxation does not lead to the formation of a new bond; relaxation energies are modest and show only a very weak dependence on the system size (see Table I). Altogether, for the removal of an O(2) or O(3) atom from the surface at least 1.75 eV more energy is required than for the creation of an O(1) vacancy.

If molecular instead of atomic oxygen is taken as a reference, half of the molecular binding energy (3.13 eV) has to be subtracted from our vacancy formation energies, leading to values ranging from 1.59 to 1.70 eV, depending on the vacancy concentration (supercell size), to be compared with experimental estimates of 1.3–1.5 eV.[19] Given the uncertainty in the experimental values and the tendency of DFT calculations to overestimate binding energies, the agreement is rather encouraging.

Since the (010) surface was widely studied, it is interesting to compare results obtained by different groups—see Table II. Ganduglia-Pirovano and Sauer[13] performed calculations using the VASP code but with slightly different settings (different plane wave energy cutoffs, different *k*-point meshes, different routines for structural relaxation, and different convergence criteria for total-energy minimization). In fact, an important difference exists already in the description

TABLE II. Comparison of three DFT studies of oxygen vacancy formation on the (010) surface of $V_2O_5$. $E_{relax}$ and $E^R_{f(O)}$ are the relaxation energies and the vacancy formation energies for relaxed surfaces, respectively. All values are in eV and take the total energy of atomic oxygen in the gas phase as reference.

| | Our results, (1×2×2) cell | | Ref. 13 | | Ref. 37 | |
|---|---|---|---|---|---|---|
| O active site | $E_{relax}$ | $E^R_{f(O)}$ | $E_{relax}$ | $E^R_{f(O)}$ | $E_{relax}$ | $E^R_{f(O)}$ |
| O(1) | −1.79 | 4.83 | −1.83 | 5.08 | −0.69 | 6.47 |
| O(2) | −1.37 | 6.88 | −1.41 | 6.81 | −0.76 | 7.19 |
| O(3) | −0.64 | 7.42 | −0.46 | 7.07 | −0.52 | 6.49 |

of the bulk crystal structure where GP reported a lattice parameter $c$ which is 0.47 Å larger than our corresponding value of $b$, indicating a significantly weaker interlayer relaxation, and lattice parameter $a$, which is 0.10 Å smaller (note that $b$ and $c$ are interchanged in the two studies). Our results are in good agreement with other calculations using both VASP (Ref. 29) and other codes.[30] Since the calculations in Ref. 13 were carried out using a $(1\times2\times2)$ supercell, the comparison in Table II refers to our results obtained with the M cell. Good agreement is found for O(2) vacancy creation (although for the medium-size cell, convergence with respect to cell size is not yet achieved.), while for the O(1) vacancy we predict a lower and for the O(3) site a higher vacancy formation energy. The different results for the O(1) vacancy are evidently related to the differences in the calculated interlayer spacing because the interaction of the undercoordinated V atoms with an O(1) atom across the interlayer gap requires a stronger distortion of the environment of the $V^*$ atom. On the other hand the distortion around an O(3)-type vacancy leads to a tensile strain on V–O bonds extending mainly along the a direction where a slightly smaller lattice constant was calculated by Ganduglia-Pirovano and Sauer.[13] A more detailed analysis is impossible because no details of the lattice distortions around O(2) and O(3) vacancies were reported in Ref. 13. Vacancy formation energies were also estimated in cluster calculations.[37] They lead to a completely different energetic hierarchy for unrelaxed structures—formation of O(3) vacancies being favored over O(1) vacancies. Upon relaxation, the vacancy formation energy for O(1) was slightly lower than for O(3) by 0.02 eV. This illustrates the limitations of a cluster approach—the energies of O(3) vacancies were poorly described due to the location of the O(3) atoms too close to the cluster edge.

Ganduglia-Pirovano and Sauer[13] also used the thermodynamic formalism based on the grand-canonical ensemble (see Sec. II B) to estimate the stability of the reduced (010) surface of $V_2O_5$ as a function of the chemical potential of oxygen. It was demonstrated that the chemical potential at which a reduced surface with O(1) vacancies is stabilized against reoxidation is comparable with the value for an incipient reduction in $V_2O_5$ to $VO_2$. We will examine the stability of the reduced surfaces as a function of the chemical potential of oxygen after presenting the results for the other low-index surfaces.

Some attempts to investigate the influence of post-DFT corrections on vacancy formation on the $V_2O_5(010)$ surface appeared very recently in the literature. Blum *et al.*[38] used periodic DFT+$U$ calculations (with an on-site Coulomb repulsion of $U=3$ eV added to the DFT Hamiltonian) to calculate the stability and electronic density of states (DOS) of a $V_2O_5(010)$ surface with O(1)-type vacancies. No vacancy formation energies were reported, but the supporting information stated that the transition between a reduced $V_2O_5$ surface and a $V_6O_{13}$ surface occurs at a value of the oxygen chemical potential of −1.6 eV (measured relative to one half of the binding energy of molecular oxygen). This is only slightly higher than the limiting value for the stability limit of reduced $V_2O_5(010)$ derived in Ref. 13. Cluster calculations using a hybrid functional presented by Sauer and Döbler[39] showed that the energies for the dissociation of the V=O bond in a vanadyl group calculated with hybrid functionals for a $V_{20}O_{62}H_{24}$ cluster are lower by about 0.6 eV than those obtained with a gradient-corrected DFT functional. However, given the different V:O ratio in the cluster and in the bulk oxide, this result must be considered with some caution. One should also note that the vacancy formation energy (~1.2 eV) derived from the hybrid-functional calculations lies as far below the experimental value [1.3–1.5 eV (Ref. 26)] as our DFT generalized gradient approximation (GGA) result overshoots experiment. A lower formation energy would stabilize the vacancy against reoxidation (at least at sufficiently reducing conditions), but a reduction by this amount would be by far not sufficient to stabilize O(2) or O(3) vacancies.

### H. Reduced (001) surface structure and energies

Energies for the formation of $O^t(1)$, $O^t(2)$, and $O^e(2)$ vacancies on the (001) surface are summarized in Table I; the relaxed surface geometries are shown in Fig. 3. An extensive relaxation is the result of the interaction between s layers [perpendicular to the (001) surface] induced by rebonding after vacancy creation. The largest relaxation energy found for the M cell is a consequence of the periodic setup since the bonding between undercoordinated $V^*$ atoms and O(1) atoms from a neighboring s layer couples pairs of layers. In this case supercells with an even number of s layers impose fewer constraints to relaxation. The S cell containing only a single s layer is evidently too small for a proper description of vacancy formation: repulsive vacancy-vacancy interactions lead to very large vacancy formation energy in the absence of relaxation; the smallness of the cell also permits only an insufficient relaxation.

At the (001) surface there is no clear site preference for vacancy creation—for the L cell, the vacancy formation energies for different oxygen sites differ by only 0.05 eV; all energies are lower by about 1 eV than for the (010) surface. Vacancy formation on the (001) surface always leads to the formation of bonds between s layers. As illustrated in Fig. 3, creation of an O(1) vacancy causes the formation of a bond between the coordinatively unsaturated $V^*$ atom and an oxygen atom from a vanadyl group in the next layer. The relaxation pattern is similar to that reported for $O^t(1)$ vacancies on the (010) surface, except that the O-$V^*$-O bridge is now parallel and not perpendicular to the surface. However, on the (001) surface, in addition, a weak bond between a V atom linked to $V^*$ by a bridging $O^t(2)$ atom and a neighboring vanadyl group from the next s layer is formed. The V–O bond lengths in the stronger link are 1.77 and 1.81 Å [i.e., comparable to the V–O(2) distance in the bulk]; while in the weaker link they are more asymmetric, 1.70 and 1.93 Å. The stronger bonds couple the s layers into pairs which are in turn connected by weaker links. For a medium $(1\times2\times4)$ cell extended zigzag chains of alternating strong and weak interplanar links are formed (see Fig. 3), while in a large $(1\times3\times4)$ cell only the three layers within the same cell are coupled explaining the slightly reduced relaxation energy. The $O^t(1)$ atoms that are not involved in the interlayer bonds move up and away from the surface, so the vanadyl double

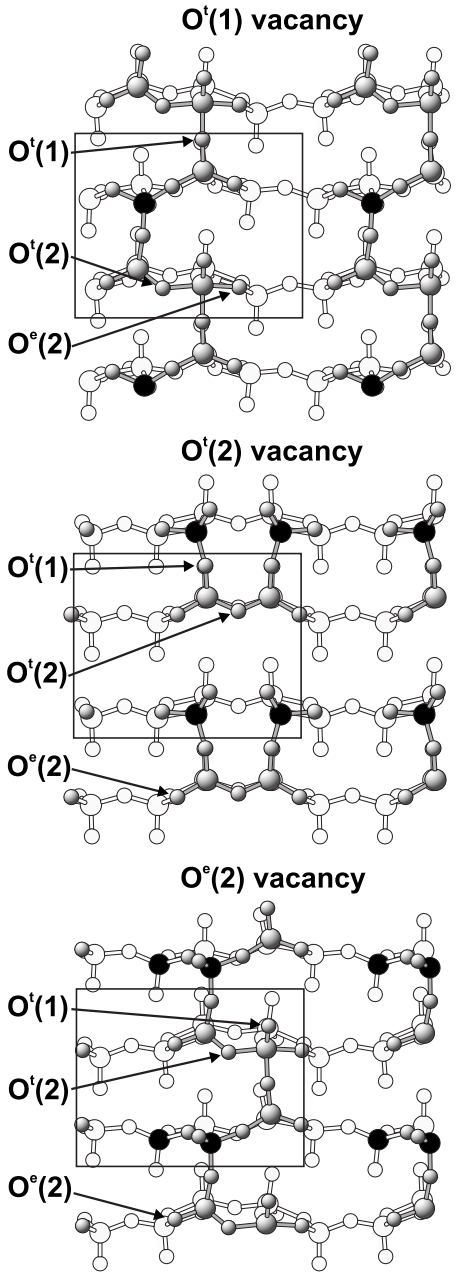


FIG. 3. Oxygen vacancies at the O(1), O(2), and O$^e$(2) sites on the (001) surface (for M supercell). Atoms from deeper subsurface layers are all depicted as white circles to emphasize surface reconstruction. For clarity, V$^*$—the vanadium atoms which were bonded to the removed O atom are depicted in solid black.

bonds form an angle of 40° with respect to the surface plane.

Removal of an O$^t$(2) oxygen atom from the plateau generates two coordinatively unsaturated V$^*$ atoms which form interlayer bonds with vanadyl groups in the neighboring s layer [see Fig. 3(b)]. The V-O$^t$(1) groups involved in these bonds do not loose completely their vanadyl character; thus the V–O bond lengths on both sides are slightly different: 1.74 and 1.86 Å. The V$^*$-O$^t$(1)-V link is also not linear, as for the O$^t$(1) vacancy, but forms an angle of 141°. Similar to O$^t$(1) vacancy formation, the remaining vanadyl groups are canted with respect to the surface plane with an angle of 43°.

The O$^e$(2) vacancy at the edge of the plateau leads to the formation of only one coordinatively unsaturated V$^*$ atom and the resulting relaxation pattern is very similar to that described for O$^t$(1) vacancy. For medium cell a zigzag chain of interlayer bonds is built (see Fig. 2) with V–O bond lengths of 1.77 and 1.79 Å for the stronger link (involving the V$^*$ atom) and 1.71 and 1.93 Å for the weaker link. The O$^t$(1) atoms in close vicinity of V$^*$ move up considerably, and the vanadyl bonds form an angle of 81° with the surface plane (see Fig. 2, bottom). Also other O$^t$(1) atoms shift upward and the corresponding vanadyl bonds form angles of approximately 42° with the surface plane. Due to the canting of the V–O(1) bonds, these oxygen atoms are more easily accessible from above the surface. This suggests that the formation of O$^e$(2)-O$^t$(1) vacancy pairs as energetically favored.

### I. Reduced (100) surface structure and energetics

Energies for the formation of O(1) and O(2) vacancies on the (100) surface are collected in Table I and the relaxed surface geometries after vacancy formation are depicted in Fig. 4. Vacancy formation on this surface is in many aspects very similar to the (001) surface. Again a strong surface relaxation is found except for the small $(1\times1\times1)$ supercell that imposes too many constraints. Larger supercells allow an independent deformation of neighboring s layers and the relaxation energy strongly increases with the size of the supercell.

For O(1) and O(2) vacancies the formation energies are 3.46 and 3.19 eV with respect to atomic oxygen and only 0.33 and 0.06 eV with respect to molecular oxygen—these are the lowest values for all low-index $V_2O_5$ surfaces. Removal of an O(1) atom results (as observed for the other surfaces) in the creation of bonds between s layers (see Fig. 4). The V$^*$-O(1)-V link is straight and parallel to the surface and consists of two single bonds with lengths of 1.84 and 1.73 Å for V$^*$-O(1) and V–O(1), respectively. The surrounding of the coordinatively unsaturated V$^*$ atom is also distorted. The V$^*$-O(2) bond length is reduced to 1.68 Å, whereas the V–O(2) distance increases to 2.26 Å (compared to 1.89 Å for the defect-free surface). In addition, a weaker bond is formed by the V atom linked by an O(2) atom to the V$^*$ site and a vanadyl group from the third s layer. This link is slightly asymmetric (bond lengths of 1.93 and 1.71 Å), and the V–O(1)–V angle is 153°. Similarly to the (001) surface, O(1) atoms, which are not involved in interlayer links, move out from the surface—the vanadyl bonds form an angle of 51° with the surface.

Formation of an O(2) vacancy leads to the creation of two coordinatively unsaturated V$^*$ atoms. In the L supercell both atoms form V$^*$-O(1)-V bridges with vanadyl oxygen atoms in the next s layer (with bond lengths of 1.83 and 1.75 Å). The bridges are no longer straight: the V$^*$-O(1)-V angle is equal to 169°. The O(1)–O(1) distance between the bridging oxygen is reduced by 1.07 Å compared to the defect-free surface. The relaxation pattern has mirror symmetry in the L cell, with pairs of V$^*$-O(1)-V bridges being separated by undisturbed vanadyl groups. This explains the increase in the

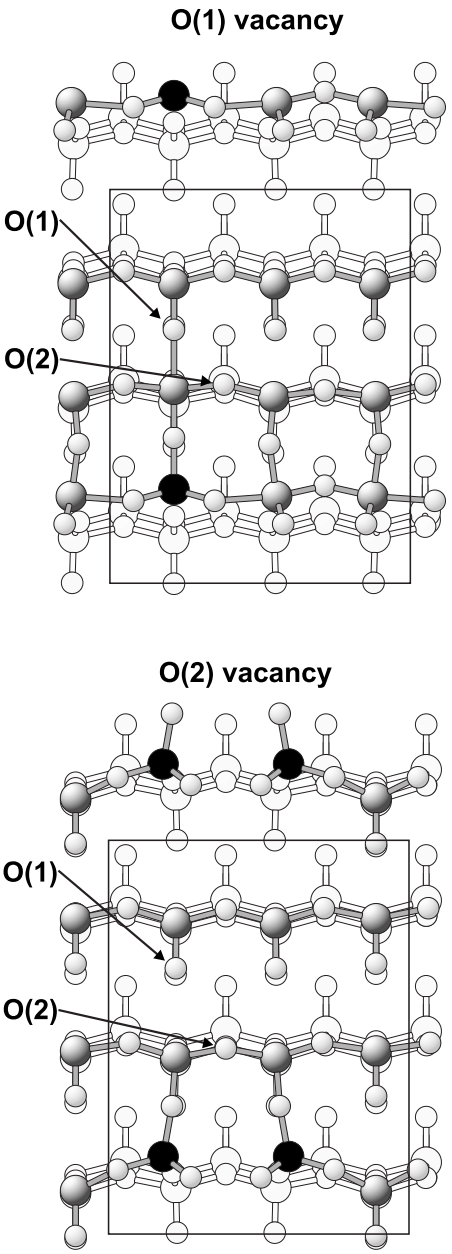


FIG. 4. Relaxed surface structure around oxygen vacancies on the (100) surface (for L supercell). Top views of the surface after removing one O(1) or O(2) oxygen atom per supercell are shown. Atoms from deeper subsurface layers are all shown as white circles. Vanadium and oxygen atoms are represented by large and small gray circles, respectively. For clarity, V*—the vanadium atoms which were bonded to the removed O atom are depicted in solid black.

relaxation energy with respect to the M cell, where the distortion fields from neighboring cells overlap. The O(1) atoms not involved in interlayer bonds again move above the surface (the angle with respect to the surface is 59°).

### J. Thermodynamic stability of the reduced surfaces

The thermodynamic formalism in the grand-canonical ensemble described in Sec. II B may be used to examine the stability of the reduced surfaces as a function of the chemical potential of oxygen above the surface. The change in the surface free energy due to the creation of a single vacancy is given (approximating again the Gibbs free energy of the stoichiometric and reduced surfaces by the DFT total energies calculated for the slabs) by

$$\Delta\gamma(T,p) = [E_{\mathrm{slab}}(N_{\mathrm{V}},N_{\mathrm{O}}-1) - E_{\mathrm{slab}}(N_{\mathrm{V}},N_{\mathrm{O}}) + \mu_{\mathrm{O}}(T,p)]/A. \tag{8}$$

Taking the binding energy of molecular oxygen as the standard for the chemical potential of oxygen, $\mu_{\mathrm{O}}(T,p) = \Delta\mu_{\mathrm{O}}(T,p) + \frac{1}{2}E(\mathrm{O}_2)$, one finds that the change in the surface free energy is given by

$$\Delta\gamma(T,p) = [E_f^{1/2\mathrm{O}_2}(\mathrm{O}) + \Delta\mu_{\mathrm{O}}(T,p)]/A, \tag{9}$$

where $E_f^{1/2\mathrm{O}_2}$ (O) is the vacancy formation energy measured relative to molecular oxygen (as listed Table I) and $\Delta\mu_{\mathrm{O}}$ is the excess chemical potential bounded below by the value where $V_2O_5$ becomes unstable against reduction to $VO_2$; $\Delta\mu_{\mathrm{O}}=-1.71$ eV as calculated according to Eq. (3) from the cohesive energies of the vanadium oxides. At a given value of the chemical potential of oxygen the formation of a vacancy is favored only if $\Delta\gamma(T,p)$ is negative, i.e., if a sufficiently strong negative $\Delta\mu_{\mathrm{O}}$ overcompensates the endothermic heat of formation of a vacancy. For the (010) surface only O(1) vacancies [$E_f^{1/2\mathrm{O}_2}$ (O)=1.59 eV] are marginally stable against reoxidation, but at an even slightly more negative chemical potential the reduction starting at the surface will initiate conversion of the substrate to a lower oxide. O(2) and O(3) vacancies ($E_f^{1/2\mathrm{O}_2}$ (O)=3.34 and 3.51 eV, respectively) on the (010) surface are highly unstable against reoxidation at all allowed values of the chemical potential. This is in agreement with the results reported in Ref. 13. In contrast, on the (001) and (100) surfaces all types of vacancies [$E_f^{1/2\mathrm{O}_2}$ (O)=0.06–0.85 eV] are stable against reoxidation even at mildly oxidizing conditions. This shows that not only the formation of oxygen vacancies requires a significantly lower energy on these edge surfaces, but vacancies will also be formed at higher concentrations and they are more resistant to reoxidation.

## IV. HYDROGEN ADSORPTION AND VACANCY FORMATION BY DEHYDROXYLATION

The differences in the total energies of the stoichiometric and the reduced surfaces are only a first and rather rough measure of the ability of an oxide surface to supply oxygen atoms to a reactant. A more realistic scenario is the adsorption of a reactant at oxygen surface atoms and the subsequent desorption of the oxidized species. The simplest realization of such a process is the adsorption of atomic hydrogen, followed by the abstraction of a hydroxyl group from the surface. Yin *et al.*[12] investigated the adsorption of atomic hydrogen on the (010) surface of $V_2O_5$ and made an attempt to evaluate the energy required for the desorption of surface hydroxyl species. However, since during the desorption process no surface relaxation was permitted, their results cannot be considered as quantitatively reliable. Tokarz-Sobieraj *et*

TABLE III. Adsorption energies for atomic hydrogen on various oxygen sites of the three low-index surfaces of $V_2O_5$ and energies for the formation of an oxygen vacancy by desorption of an isolated hydroxyl group, as calculated for supercells of different size (cf. text).

| | | (010) | | | (001) | | | (100) | |
|---|---|---|---|---|---|---|---|---|---|
| Supercell | Energy | O(1) | O(2) | O(3) | O(1) | O(2) | $O^e(2)$ | O(1) | O(2) |
| S | $E^{H}_{ads}$ | −2.97 | −2.71 | −2.42 | −3.20 | −3.17 | −2.90 | −2.47 | −2.32 |
| | $E^{R}_{f(OH)}$ | 3.12 | 5.17 | 5.03 | 4.84 | 6.09 | 4.86 | 4.21 | 5.55 |
| M | $E^{H}_{ads}$ | −3.01 | −2.79 | −2.60 | −4.13 | −4.49 | −4.28 | −3.88 | −3.49 |
| | $E^{R}_{f(OH)}$ | 3.18 | 5.01 | 5.36 | 3.01 | 3.53 | 3.13 | 3.64 | 3.21 |
| L | $E^{H}_{ads}$ | −3.04 | −2.96 | −2.88 | −4.20 | −3.77 | −4.13 | −4.60 | −3.75 |
| | $E^{R}_{f(OH)}$ | 3.10 | 4.77 | 4.82 | 3.37 | 2.97 | 3.35 | 3.40 | 2.28 |

*al.*[40] performed cluster studies on the $V_2O_5$ (010) surface and concluded that creation of oxygen vacancies through desorption of water molecules is in fact exoenergetic although with a desorption barrier. Here the studies of vacancy formation by dehydroxylation were extended to other low-index surfaces, allowing a full relaxation of the surfaces with an adsorbed H atom and after OH elimination.

### A. Hydrogen adsorption on the (010) surface

Adsorption of atomic hydrogen is an exothermic process on all three low-index surfaces. The adsorption energies for atomic hydrogen calculated for different oxygen sites on the three low-index surfaces of $V_2O_5$ are summarized in Table III. We begin by discussing the results for the (010) surface where hydrogen may be adsorbed on all three different oxygen sites. The geometries of the hydroxylated surfaces are shown in Fig. 5. For clarity, on all further figures the atoms of OH group are shown in solid black.

Hydrogen is adsorbed at the O(1) atom of a vanadyl group with an O(1)–H bond length of 0.98 Å and a H–O(1)–V angle of 124°. The canting of the OH group allows to form a weak hydrogen bond with an O(2) atom (see Fig. 5). Adsorption induces an elongation of the bond length in the vanadyl group by about 0.14 Å and some smaller changes in the bond lengths between V and its in-plane O neighbors. Hydrogen adsorption on an O(2) site (see Fig. 5) leads (by symmetry) to an upright position of the OH group, with a bond length of 0.98 Å. Bonds between the O(2) site and the two V neighbors are stretched to 1.80 and 1.97 Å. Adsorption on the O(3) atom (see Fig. 5) positions the hydrogen atom rather close to the surface (bond length of 0.98 Å) and allows, through a canted OH group, the formation of two weak hydrogen bonds to the neighboring O(2) sites (which are 2.49 Å away). Out of three O(3)–V bonds, the longest (2.06 Å on the clean surface) is further stretched to 2.28 Å and the two shorter (1.90 Å on clean surface) are also elongated by 0.14 Å. The H-adsorption energies increase modestly with increasing size of the supercell because the repulsive Coulomb interactions between the hydroxyl groups are reduced. The relaxation of the substrate has a strong influence on the adsorption energies—without relaxation, adsorption on the O(1) site is strongly preferred over the other

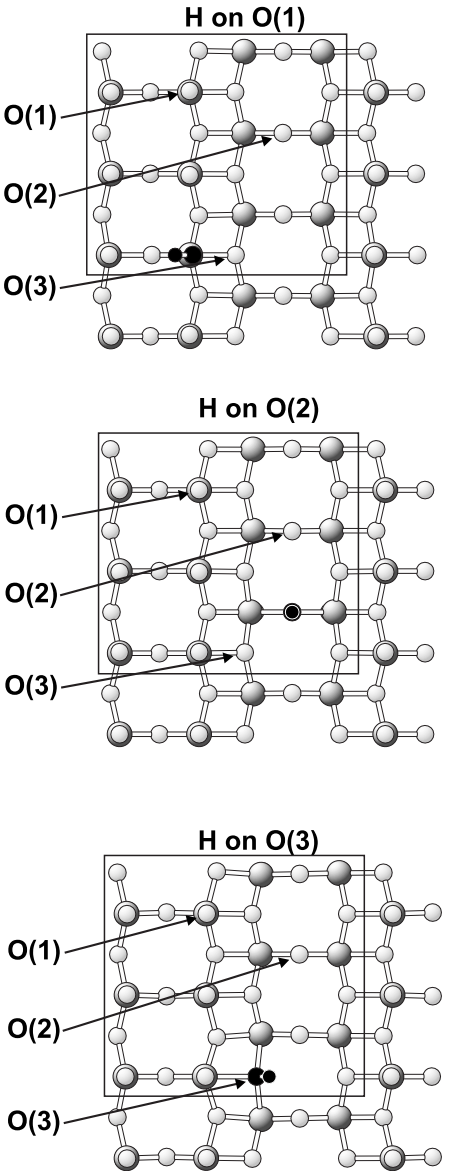


FIG. 5. Relaxed geometries after adsorption of individual hydrogen atom at oxygen active sites O(1), O(2), and O(3) on the (010) surface (for the L supercell). Vanadium atoms are represented by large gray circles and oxygen atoms by smaller gray circles. For clarity, atoms of the OH group are depicted in solid black.

oxygen sites, while including relaxation, only minor differences between adsorption sites are found (see Table III). If relaxation is ignored, our results are in reasonable agreement with those of Yin *et al.*[12] and Fu *et al.*[15]

### B. Hydrogen adsorption on the (001) surface

The conditions for the adsorption of hydrogen on the other two surfaces are more complex, especially for the O(1) sites, because here the vanadyl bonds are parallel to the surface. This also leads to a strong dependence on the supercell size: for the smallest supercell, the H-adsorption energies are by 0.6–1.3 eV less exoenergetic compared to larger supercells. A relatively high concentration of H atoms on the (001) surface prevents an efficient geometry relaxation that could lower the adsorption energy.

Adsorption of H at an O(1) site results in an O–H bond length of 0.98 Å; the OH group is tilted with respect to the surface normal by an angle of approximately 25° (see Fig. 6). The V–O(1)–H angle is 122°. Like in the case of O-vacancy formation, H adsorption facilitates the creation of interlayer bonds parallel to the surface. One bond is formed between the vanadium connected to the OH group and the O from a vanadyl group in a neighboring s layer [with V–O(1) bond lengths of 1.77 and 1.83 Å]. A similar bond is formed by a neighboring vanadium (the one without OH group), linking to another s layer (with V–O bond lengths of 1.74 and 1.90 Å)—see Fig. 6. In effect the first link couples the layers into pairs which are then connected by secondary links. In the M supercell, this establishes an uninterrupted zigzag chain of interlayer bonds. In the larger L supercell the three layers within the same supercell are coupled, but no links to their repeated images are formed. For this reason, the H-adsorption energies even slightly decrease for the larger cell (see Table III).

A strong dependence on the cell size is found for H-adsorption energies at the O(2) site (see Table III). For the M cell (see Fig. 6), geometry optimization leads to a breaking of one of the bonds of the O atom to its V neighbors and the V–O(2)–H group with vanadyl character is formed [$d$(V-O)=1.77 Å, $d$(O-H)=0.98 Å, V–O–H angle=123°]. In the L cell the V–O(2)H–V link is not broken but becomes asymmetric [with two V–O(2) bonds of 1.84 and 2.17 Å]; the O(2)–H bond is slightly elongated to 1.01 Å. For the M cell interlayer coupling [like for H adsorption at O(1)] on hydrogen adsorption is observed. Alternating links with and without the V–O(2)–H group are formed. The V–O bond lengths are 1.76 and 1.84 Å when an OH group is involved or 1.71 and 1.94 Å when it is not. In a larger supercell only one interplanar bond per cell is created. The different number of interlayer bonds per supercell is responsible for large differences in adsorption energy calculated for M ($E_{ads}^{H}$= −4.49 eV) and L ($E_{ads}^{H}$=−3.77 eV) supercells.

There are no substantial differences in the characterization of H adsorption at the $O^e(2)$ site for M and L supercells. In both cases one (in-plane) V-$O^e$(2)H bond is broken (elongated to over 3 Å) and a regular vanadyl group is formed [$d$(V-O)=1.78 Å, $d$(O-H)=0.98 Å] with an angle of 30° to the surface (see Fig. 6). Again, zigzag chains of interlayer

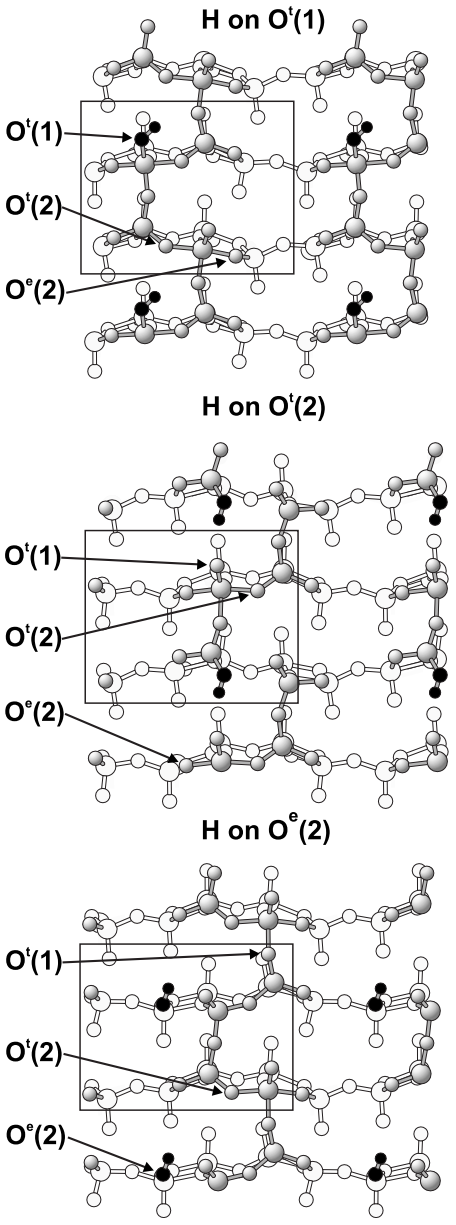


FIG. 6. Relaxed geometries after adsorption of individual hydrogen atom at the O(1), O(2), and $O^e$(2) sites on the (001) surface (for the M supercell). Atoms from deeper subsurface layers are all shown as white circles. Vanadium atoms are represented by large gray circles and oxygen atoms by smaller gray circles. For clarity, atoms of the OH group are depicted in solid black.

links are built. Slightly shorter links (V–O bond lengths 1.77 and 1.80 Å) involve the vanadium site undercoordinated due to the broken $O^e$(2)-V-OH bond described above. Longer links (V–O bond lengths 1.71 and 1.95 Å) are formed with neighboring vanadium sites. The H-adsorption energies are equal to −4.28 and −4.13 eV for M and L cells, respectively.

### C. Hydrogen adsorption on the (100) surface

Medium and large supercells yield significantly different results for hydrogen adsorption at the O(1) site on the (100) surface—the adsorption energy is larger by 0.72 eV for the

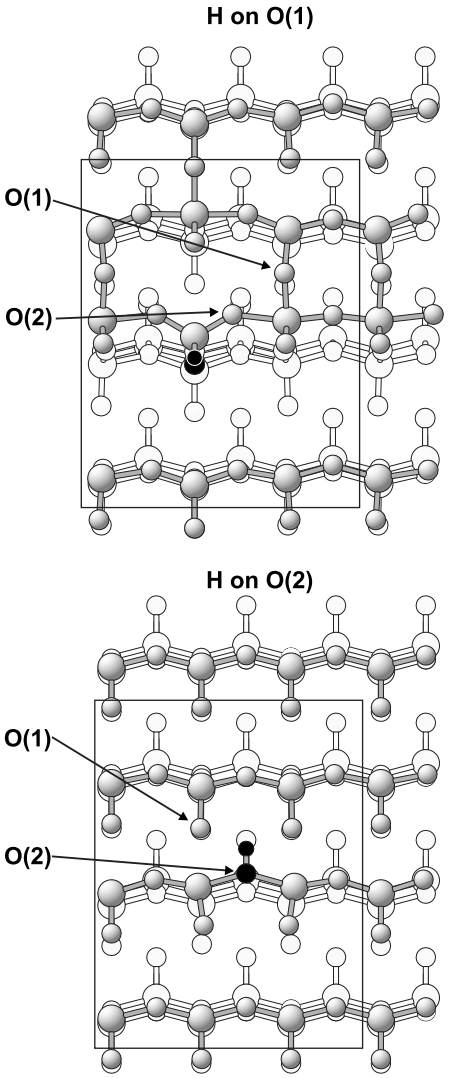


FIG. 7. Relaxed geometries for hydrogen adsorption on the (100) surface (for the L supercell). Top views of the surface after adsorption of individual hydrogen atom at the O(1) and O(2) oxygen sites are shown. Atoms from deeper subsurface layers are all shown as white circles. Vanadium and oxygen atoms are represented by large and small circles, respectively. For clarity, atoms of the OH group are depicted in solid black.

larger cell (see Table III). For the M cell the O–H bond length is slightly elongated to 1.02 Å and the V–O–H angle is 112°. The angle of O–H bond to the surface is 54°. We also find creation of a hydrogen bond between the OH group and an O(1) oxygen from a neighboring vanadyl group, with $d$(O-H)=1.68 Å, as well as formation of two weak interlayer links (with bond lengths of 2.03 and 1.67 Å and of 1.98 and 1.67 Å, respectively). For the large supercell (see Fig. 7) the O–H bond forms an angle of about 105° with the surface, the O–H bond length is 0.97 Å, and the V–O(1)–H angle is 128°. Interlayer links (with bond lengths of 1.70 and 1.92 Å) are formed between the vanadium without OH group and vanadyl group in the next s layer. The network of interlayer links is rather irregular and seems to couple the s layers in threes, but this is related to the periodicity of the L supercell. The surrounding of the vanadium atom with an OH group attached is strongly distorted; one V–O(2) bond length is reduced to 1.70 Å and the other is increased to 2.12 Å. Similar to the creation of an O(1) vacancy the relaxation energy increases monotonously with supercell size and is responsible for large differences in the hydrogen adsorption energies for medium (−3.88 eV) and big (−4.60 eV) supercells.

On the other hand, medium and large supercells give very similar results for hydrogen adsorption at O(2) site (see Fig. 7). The OH group is almost parallel to the surface (angle of 5°) and the O–H bond length is 0.98 Å. For a medium cell a weak and rather asymmetric (bond lengths of 1.66 and 2.26 Å) interlayer link is formed by a vanadium atom and a vanadyl group from a neighboring s layer. In the large cell no such links are formed. The similar geometries of the OH groups and their environment result in small differences in the hydrogen adsorption energies: −3.49 eV for M and −3.75 eV for L cells.

### D. Formation of oxygen vacancies by desorption of a hydroxyl group

The energies for desorption of an isolated hydroxyl group from one of the low-index $V_2O_5$ surfaces are collected in Table III. Obviously the desorption of OH is easier than the removal of an oxygen atom. The effect is strongest on the (010) surface where the energy required for vacancy formation is reduced by 1.62–2.24 eV, depending on the oxygen site and the size of the supercell. For the O(1) site the strong reduction by 1.62 eV (for L cell) is not unexpected since the removal of the oxygen atom from a vanadyl group requires the breaking of a strong V=O double bond, whereas only a single bond is broken upon removal of an OH group. For the O(2) and O(3) sites the reduction is even larger because the adsorption of H atoms reduces the bond strength of two or three back bonds between the O atom and the surrounding V atoms, respectively.

On the two unsaturated surfaces, adsorption of hydrogen and formation of surface OH groups also facilitates vacancy creation, but the effect is not as strong. The reduction in the vacancy formation energies, for the L cell, is in the range of 0.1–0.9 eV. The absolute values are rather similar, ranging from 2.28 to 3.40 eV, which is still by over 1 eV lower than for O(2) and O(3) vacancies on the (010) surface. Results obtained from S cells are not realistic due to serious hindering of the surface relaxation.

The (100) and (001) surfaces also differ from the saturated (010) surface by their ability to adsorb and dissociate water to create Brönsted acid sites,[8] which has a large impact on catalytic properties. Properties of different Brönsted sites at the three considered surfaces are currently being investigated.

## V. CONCLUSIONS

The stability of the three low-index surfaces of $V_2O_5$ and the formation of oxygen vacancies by desorption of atomic oxygen or via hydroxylation followed by the abstraction of the OH group on these surfaces were investigated using pe-

riodic *ab initio* DFT calculations. Surface models of three different sizes are used, corresponding to three different concentrations of surface vacancies. For the smallest supercells (with a surface periodicity equivalent to a crystallographic unit cell of $V_2O_5$) strong interactions between vacancies or hydroxyl groups and geometrical constraints limiting an efficient relaxation lead to unrealistic results, especially for the creation of vacancies at twofold or threefold coordinated oxygen sites.

On the most stable (010) surface, the vacancy formation energy is the lowest for the O(1) site (vanadyl oxygen), assisted by a large relaxation energy arising from the formation of back bonds between the V atom from which the O is removed and a vanadyl group in the subsurface layer. Formation of O(2) and O(3) vacancies is energetically less favorable (by at least 1.7 eV), although for lower vacancy concentrations the relaxation contribution is quite substantial. An important result is the finding, in agreement with Ganduglia-Pirovano and Sauer,[13] that on the (010) surface only O(1) vacancies are marginally stable at strongly reducing conditions close to those where bulk $V_2O_5$ becomes unstable against reduction to $VO_2$. On this surface O(2) and O(3) vacancies are unstable against reoxidation at all permissible values of the chemical potential.

Vacancy formation on the less stable (100) and (001) surfaces was investigated. We find that at the lowest vacancy concentration, the formation of vacancies on the (001) and (100) surfaces requires about 0.9 and 1.5 eV less energy, respectively, than the formation of an O(1) vacancy on the (010) surface. At higher vacancy concentrations, cooperative effects (more favorable relaxed structures) lead to even more pronounced differences. It is also remarkable that while on the (010) surface the formation of any type of vacancy other than O(1) is practically excluded, on the other surfaces the energies for the removal of onefold and twofold coordinated oxygens requires similar energies. The thermodynamic analysis confirms that on these surfaces all types of oxygen vacancies are stable against reoxidation over a wide range of the chemical potential of oxygen.

Our results shed a new light on the catalytic properties of $V_2O_5$. So far, it was tacitly assumed that the active sites are located only on the most stable (010) surface, the natural cleavage plane. We have shown that, although the surface energies of the unsaturated surfaces are about 1 order of magnitude higher than that of the (010) surface, in equilibrium the (001) and (100) surfaces occupy about 15% of the surface of $V_2O_5$ crystallites. Surface relaxation plays a very important role in reducing the surface energies of these edge surfaces. The formation of vacancies on these surfaces requires a substantially lower energy than on the (010) surface. In fact, on the (010) surface, vacancies can exist in chemical equilibrium with the reactive atmosphere only at oxygen partial pressures low enough to almost destabilize the bulk crystal against decomposition to $VO_2$ and $O_2$. In contrast, oxygen vacancies on other surfaces are stable even at significantly higher partial pressures of oxygen.

The conclusions based on the energies for oxygen removal are confirmed by the investigation of hydrogen adsorption and vacancy formation by the removal of hydroxyl groups. In general, this process requires substantially less energy than the removal of an oxygen atom. On the (010) surface formation of O(1) vacancies remains strongly favored, while on the (001) and (100) surfaces, the formation of O(2)-type vacancies requires even less energy. Although the anisotropy of the vacancy formation energies is less pronounced if a hydrogen-assisted process is considered, the result that the reduced (010) surface will be fully reoxidized already at lower values of the oxygen chemical potential than other surfaces remains important.

In conclusion, we have demonstrated that the surface area of $V_2O_5$ crystallites contains a non-negligible fraction of low-index surfaces other than (010) (the natural cleavage plane). The formation of oxygen vacancies on these surfaces requires considerably less energy than vacancy formation on the (010) surface, and vacancies on the (100) and (001) surfaces are also stable against reoxidation under not too strongly oxidizing conditions. One may expect that these findings will considerably modify the scenario for catalytic oxidation on $V_2O_5$.

## ACKNOWLEDGMENTS

J.G. acknowledges support from the Marie-Curie Training Site "Atomic Scale Computational Materials Science" at the Universität Wien. J.H and R.G. acknowledge support from Austrian Science Funds (Project No. P19983-N16). M.W. acknowledges support from the Polish Ministry of Science and High Education (Grant No. N204 024 31/0475).

*Corresponding author; ncgrybos@cyf-kr.edu.pl

[1] P. Mars and D. W. van Krevelen, Spec. Suppl. Chem. Eng. Sci. **3**, 41 (1954).
[2] J. Haber, M. Witko, and R. Tokarz, Appl. Catal., A **157**, 3 (1997), and references therein.
[3] D. W. Blakely and G. A. Somorjai, J. Catal. **42**, 181 (1976).
[4] J. Ziółkowski, J. Catal. **80**, 263 (1983).
[5] J. C. Volta and J. L. Portefaix, Appl. Catal. **18**, 1 (1985).
[6] J. C. Volta and J. M. Tatibouet, J. Catal. **93**, 467 (1985).
[7] M. Gąsior and T. Machej, J. Catal. **83**, 472 (1983).
[8] M. Gąsior and B. Grzybowska, React. Kinet. Catal. Lett. **32**, 281 (1986).
[9] R. L. Smith, W. Lu, and G. S. Rohrer, Surf. Sci. **322**, 293 (1995).
[10] R. L. Smith, G. S. Rohrer, K. S. Lee, D.-K. Seo, and M. K. Whangbo, Surf. Sci. **367**, 87 (1996).
[11] Ch. Mathieu, S. Peralta, and A. Da Costa, and Y. Barbaux, Surf. Sci. **395**, L201 (1998).
[12] X. Yin, H. Han, A. Endou, M. Kubo, K. Teraishi, A. Chatterjee, and A. Miyamoto, J. Phys. Chem. B **103**, 1263 (1999).
[13] M. V. Ganduglia-Pirovano and J. Sauer, Phys. Rev. B **70**, 045422 (2004).

[14] M. V. Ganduglia-Pirovano and J. Sauer, J. Phys. Chem. B **109**, 374 (2005).
[15] H. Fu, Z.-P. Liu, Z. H. Li, W. N. Wang, and K. N. Fan, J. Am. Chem. Soc. **128**, 11114 (2006).
[16] G. Kresse and D. Joubert, Phys. Rev. B **59**, 1758 (1999).
[17] J. P. Perdew, J. A. Chevary, S. H. Vosko, K. A. Jackson, M. R. Pederson, D. J. Singh, and C. Fiolhais, Phys. Rev. B **46**, 6671 (1992).
[18] S. Grimme, J. Comput. Chem. **24**, 25 (2004); **27**, 1787 (2007).
[19] T. Kerber, M. Sierka, and J. Sauer, J. Comput. Chem. **29**, 2088 (2008).
[20] M. V. Ganduglia-Pirovano, A. Hofmann, and J. Sauer, Surf. Sci. Rep. **62**, 219 (2007).
[21] A. Rohrbach, J. Hafner, and G. Kresse, Phys. Rev. B **69**, 075413 (2004); **70**, 125426 (2004).
[22] C. Franchini, V. Bayer, R. Podloucky, J. Paier, and G. Kresse, Phys. Rev. B **72**, 045132 (2005).
[23] M. Finnis, Phys. Status Solidi A **166**, 397 (1998).
[24] K. Reuter and M. Scheffler, Phys. Rev. B **65**, 035406 (2001).
[25] G. Wulff, Z. Kristallogr. **34**, 449 (1901).
[26] P. Kofstad, *Nonstoichiometry, Diffusion, and Electrical Conductivity in Binary Metal Oxides* (Wiley, New York, 1972).
[27] H. G. Bachmann, F. R. Ahmed, and W. H. Barnes, Z. Kristallogr. **ll5**, 110 (1961).
[28] R. Enjalbert and J. Galy, Acta Crystallogr., Sect. C: Cryst. Struct. Commun. **42**, 1467 (1986).
[29] G. Kresse, S. Surnev, M. G. Ramsey, and F. P. Netzer, Surf. Sci. **492**, 329 (2001).
[30] J. S. Braithwaite, C. R. A. Catlow, J. D. Gale, and J. H. Harding, Chem. Mater. **11**, 1990 (1999).
[31] J. Goclon, R. Grybos, M. Witko, and J. Hafner, J. Phys.: Condens. Matter **21**, 095008 (2009).
[32] N. V. Hieu and D. Lichtman, J. Vac. Sci. Technol. **18**, 49 (1981).
[33] S. F. Cogan, N. M. Nguyen, S. J. Perotti, and R. D. Rauh, J. Appl. Phys. **66**, 1333 (1989).
[34] A. Z. Moshfegh and A. Ignatiev, Thin Solid Films **198**, 251 (1991).
[35] M. V. Bollinger, J. V. Lauritsen, K. W. Jacobsen, J. K. Nørskov, S. Helveg, and F. Besenbacher, Phys. Rev. Lett. **87**, 196803 (2001).
[36] M. V. Bollinger, K. W. Jacobsen, and J. K. Nørskov, Phys. Rev. B **67**, 085410 (2003).
[37] K. Hermann, M. Witko, R. Druzinic, and R. Tokarz, Appl. Phys. A: Mater. Sci. Process. **72**, 429 (2001).
[38] R. P Blum, H. Niehus, C. Hucho, R. Fortrie, M. V. Ganduglia-Pirovano, J. Sauer, S. Shaikhutdinov, and H. J. Freund, Phys. Rev. Lett. **99**, 226103 (2007).
[39] J. Sauer and J. Döbler, Dalton Trans. **2004**, 3116.
[40] R. Tokarz-Sobieraj, M. Witko, and R. Grybos, Catal. Today **99**, 241 (2005).